Inviscid Instability Analysis of Triple Flames

By Qianlong Liu

November 7, 2001

Department of Mechanical Engineering, University of California, Berkeley, Berkeley, CA 94720-1740, USA

In partial fulfillment of Master of Engineering

under the supervision of Prof. J.-Y. Chen

Abstract

The stability of flames is of great importance to the practices of combustion devises. Triple flames are an important feature seen in partially premixed systems which are used for many low emission combustors. Buoyancy can play a key role in many laminar flames, such as nonpremixed jet flames. An inviscid analysis of triple flames under the influence of gravity is performed to identify the most amplified frequency in a spatially developing flow. Favorable comparisons are found between the theoretical results and those observed in numerical simulations.

1 Introduction

Since the work of Phillips (1965) [1] more than three decades ago, there has been a growing interest in the study of triple flames (Buckmaster and Matalon [2], Hartley and Dold [3], Chung and Lee [4], Kioni et al. [5], Lee et al [6], Lee and Chung [7], Ruetsch et al [8], Ruetsch and Ferziger [9],

Domingo and Vervisch [10], Plessing et al [11], Daou and Liñán [12], Echekki and Chen [13], Ghosal and Vervisch [14]). The interest is largely motivated by the potential role these structures play in the burning of partially-premixed mixtures, especially for the stabilization and ignition in diffusion flames (e.g., Phillips 1965 [1], Chung and Lee [4], Im and Chen [16],Chen and Bilger [15]).

Prediction of the characteristics of chemically reacting mixing layers is very important for a number of technologies. For the purpose of mixing enhancement, we prefer to have turbulent flows, which occur only if the laminar flows become unstable. Therefore, it is important to analyze the stability of reacting flows. Linear stability analysis is the most convenient tool for this purpose. The stability of nonreacting mixing layers has been extensively investigated. In most of previous work, analytic mean velocity profiles(usually hyperbolic tangent or error functions) were used. The validity of doing so has been investigated by Shin and Ferziger [17].

For incompressible parallel inviscid flows, Rayleigh [18] showed that, if the velocity profile has an inflection point, the flow may be unstable. Lin [19] suggested that the inviscid mechanism dominates at large Reynolds numbers with viscosity producing only slight damping. Michalke [20] numerically integrated the Rayleigh stability equation with the hyperbolic-tangent velocity profile for temporally as well as spatially growing disturbances to incompressible flow; the spatial case results agreed well with experiments. The effects of the mean velocity profile were studied by Monkewitz and Huerre [21], who found that the amplification rate found with the Blasius mixing layer velocity profile agreed well with experimental results. Morkovin [22] suggested that only stability analyses based on mean profiles derived from the boundary-layer equations should be compared with experimental results; this is consistent with Michalke's proposition. Koochesfahani and Frieler [23] investigated the linear spatial stability of plane mixing layers with both uniform and non-uniform density; they used analytical profiles. Kimura [24] constructed a stability theory for axisymmetric parallel flows and showed that the oscillation of laminar-jet flames can be explained by linear stability analysis. Trouve and Candel [25] performed a linear stability analysis of the inlet jet in a ramjet dump combustor using hyperbolic-tangent velocity and temperature profiles. They found that the density variation has a significant effect in the instability. Jackson and Grosch [26] studied the effect of heat

release in the spatial stability of a supersonic reacting mixing layer using the hyperbolic-tangent velocity profile and the flame sheet approximation. Recently, Mahalongam et al [27], studied the effects of heat release on the stability of coflowing, chemically reacting jets. They suggested that the heat release due to chemical reaction stabilizes the flow.

For compressible flows, Groppengiesser [28] used laminar solutions of the compressible boundary-layer equations as the base flow and found a second mode of instability at high Mach number, which was subsequently rediscovered by Blumen et al [29]. Sandham and Reynolds [30] solved the linearized inviscid compressible stability equation and found maximum amplification at the frequency at which vortices are found in the laboratory. They also found that three-dimensional effects are important at high Mach number. Buckmaster and Peter [31] performed an inviscid linear instability analysis for a candle flame. The results are comparable with experimental results.

In this report, we consider a low-speed, two-dimensional triple flame in which fuel and oxidizer are partially mixed at the inlet. First, the governing equations and the linear stability formulation are given and reduced for two-dimensional flows. Second, detailed discussions of the linear stability analysis are presented including the boundary conditions, the characteristics of eigenfunction for symmetric flows, and the numerical solution techniques. Third, the numerical tools developed here are validated against previously published results. Then, numerical calculations of instability equations were conducted for analytically specified profiles as well as for those fit to numerical results. The predicted frequency of the most amplified mode is then compared to that observed in numerical simulations of triple flames. Finally, a summary of the results is presented.

2 Inviscid Stability Eigenfunction Equations

The general formulation developed below can be applied to premixed, non-premixed, and triple flames in two-dimensional planar shear layers. It is assumed that the flow is parallel with its predominant flow direction parallel to the x-axis. The parallel flow assumption implies that the predominant variation of the mean flow properties varies in the direction normal to the

flow. In the linear stability analysis to be described below, all flow variables, such as density ρ, velocities u and v, pressure p, and temperature T, are assumed to be the sum of the mean and disturbance components and can be represented by the form:

$$f(x, y, t) = \bar{f}(y) + f'(x, y, t), \tag{1}$$

where $f(x, y, t)$ is a generic flow variable that is a function of position and time. The over-bars and primes denote the mean and disturbance components, respectively. Because the parallel flow assumption is invoked, $\bar{f}$ is assumed to vary only with the cross-stream co-ordinate y.

It is further presumed that any general disturbance represented by the primed variables can be constructed by the form of traveling wave disturbances:

$$f'(x, y, t) = \tilde{f}(y) exp[i(\alpha x - \beta t)], \tag{2}$$

where the quantity $\tilde{f}(y)$ is the eigenfunction assumed to be a function of y only, α is the complex streamwise wave number, β is the given temporal frequency, and i is defined by $i \equiv \sqrt{-1}$. For the temporal stability analysis, α is real and β is complex, whereas for the spatial stability analysis, α is complex and β is real. The amplification rates for the two cases are β_i and $-\alpha_i$, respectively.

Starting from the governing equations for continuity, momentum, and energy, and the ideal gas state equation of a heat-conducting viscous fluid under the action of gravity, we simplify these equations for two-dimensional, inviscid, low Mach number, and parallel flows and obtain the non-dimensional equations. The disturbance equations are derived by substituting Eq.(1) into the non-dimensional equations and then neglecting the products of disturbances to linearize them. The eigenfunction equations are derived by substituting Eq.(2) into the linearized disturbance equations.

2.1 Governing Equations

The equations of motion of a heat-conducting viscous fluid under the action of gravity can be found in textbooks. In the notation of Cartesian tensors with position vector x_j and velocity u_j $(j = 1, 2, 3)$, the exact equations are as follows.

The equation of continuity is

$$\frac{\partial \rho}{\partial t} + \frac{\partial (\rho u_j)}{\partial x_j} = 0, \tag{3}$$

where ρ is the density of the fluid.

The equations of motion, or of momentum, are the Navier-Stokes equations,

$$\rho \frac{Du_i}{Dt} = -g\rho\delta_{i3} + \frac{\partial \sigma_{ij}}{\partial x_j}, \tag{4}$$

where $\frac{D}{Dt} = \frac{\partial}{\partial t} + u_j \frac{\partial}{\partial x_j}$, the x_3-axis is the upward vertical, and the stress tensor is given by

$$\sigma_{ij} = -p\delta_{ij} + \mu \left(\frac{\partial u_i}{\partial x_j} + \frac{\partial u_j}{\partial x_i} - \frac{2}{3} \frac{\partial u_k}{\partial x_k} \delta_{ij} \right) + \lambda \frac{\partial u_k}{\partial x_k} \delta_{ij},$$

where p is the pressure, μ is the coefficient of dynamic viscosity of the fluid, and λ is the bulk viscosity, or second viscosity.

The equation of energy, or of heat conduction, is

$$\rho \frac{De}{Dt} = \frac{\partial}{\partial x_j} \left(k \frac{\partial T}{\partial x_j} \right) - p \frac{\partial u_j}{\partial x_j} + \Phi - Q_F \omega_F, \tag{5}$$

where e is the internal energy per unit mass of the fluid, k is the thermal conductivity, T is the temperature, Q_F is the heat of reaction per unit mass of fuel burned, ω_F is the chemical reaction rate of fuel, and the rate of viscous dissipation per unit volume of fluid is given by

$$\Phi = \frac{1}{2}\mu \left(\frac{\partial u_i}{\partial x_j} + \frac{\partial u_j}{\partial x_i} \right)^2 + \left(\lambda - \frac{2}{3}\mu \right) \left(\frac{\partial u_k}{\partial x_k} \right)^2.$$

For a calorically perfect gas $e = c_v T$, where c_v is the specific heat at constant volume and T is the absolute temperature.

The ideal gas state equation is

$$p = \rho R T, \tag{6}$$

where p is the absolute pressure, ρ is the density, T is the absolute temperature, and $R = R_u/M$ is the specific gas constant which is a different value for different gases. R_u is the universal gas constant, i.e., the same for all gases, and M is the molecular weight of the gas.

2.2 Simplified Equations

For two-dimensional inviscid flows without the action of gravity, we have the following properties: $w(x, y, t) = 0$, $\mu = 0$, $\lambda = 0$, and $g = 0$. Neglect of both viscosity and buoyancy has been used by Buckmaster and Peters [31] and they concluded that both of these terms are of the same order. For consistency, both viscosity and buoyancy should be excluded from the inviscid analysis. Inviscid results also justify the approximation that the effects corresponding to the chemical reaction rate are small, except for their influence on the mean flow via density change. This approximation has been justified by Mahalongam et al [27]. Therefore, we can simplify the above governing equations as following:

$$\frac{\partial \rho}{\partial t} + \frac{\partial \rho u}{\partial x} + \frac{\partial \rho v}{\partial y} = 0, \tag{7}$$

$$\rho \left(\frac{\partial u}{\partial t} + u\frac{\partial u}{\partial x} + v\frac{\partial u}{\partial y} \right) = -\frac{\partial p}{\partial x}, \tag{8}$$

$$\rho \left(\frac{\partial v}{\partial t} + u\frac{\partial v}{\partial x} + v\frac{\partial v}{\partial y} \right) = -\frac{\partial p}{\partial y}, \tag{9}$$

$$\rho \frac{De}{Dt} = \frac{\partial}{\partial x_j} \left(k\frac{\partial T}{\partial x_j} \right) - p\frac{\partial u_j}{\partial x_j}, \tag{10}$$

$$p = \rho RT. \tag{11}$$

Let us now obtain a form of the energy equation in terms of enthalpy h only. By definition of enthalpy,

$$h = e + pv = e + \frac{p}{\rho},$$

which suggests that

$$\rho \frac{De}{Dt} = \rho \frac{Dh}{Dt} - \frac{Dp}{Dt} + \frac{p}{\rho}\frac{D\rho}{Dt}. \tag{12}$$

From the equation of continuity, Eq.(7), we have

$$\frac{D\rho}{Dt} = -\rho \frac{\partial u_j}{\partial x_j}. \tag{13}$$

Substituting Eq.(13) into (12) and then into the energy equation, Eq.(10), we have

$$\rho c_p \frac{DT}{Dt} = \rho \frac{Dh}{Dt} = \frac{\partial}{\partial x_j}\left(k\frac{\partial T}{\partial x_j}\right) + \frac{Dp}{Dt} \approx \frac{\partial}{\partial x_j}\left(k\frac{\partial T}{\partial x_j}\right),$$

that is,

$$\rho c_p \frac{DT}{Dt} \approx \frac{\partial}{\partial x_j}\left(k\frac{\partial T}{\partial x_j}\right), \tag{14}$$

where the enthalpy $h = c_p T$ for the thermally perfect gas, c_p is the specific heat at constant pressure, T is the absolute temperature, and $p \approx constant$ for parallel flows. Therefore, Eqs.(7), (8), (9), (14), and (11) consist of the equations for continuity, momentum, and energy, and the ideal gas state equation for two-dimensional, inviscid, low Mach number, and parallel flows.

2.3 Dimensionless Equations

It is convenient, as usual, to write the governing equations in terms of dimensionless quantities, and for this purpose we introduce the characteristic length L, velocity V, density ρ_0, and temperature T_0 of the fluid. Their choices are, of course, problem dependent. If we now let

$$t_* = tV/L, x_* = x/L, y_* = y/L, u_* = u/V,$$

$$v_* = v/V, p_* = p/(\rho_0 V^2), \rho_* = \rho/\rho_0, T_* = T/T_0, \tag{15}$$

and substitute the transformation, Eq.(15), into the governing equations, Eqs.(7), (8), (9), (14), and (11). Denoting dimensionless quantities as the notations without the subscript $*$, we obtain the dimensionless equations for continuity, momentum, and energy, and the equation of state as

$$\frac{\partial \rho}{\partial t} + \frac{\partial \rho u}{\partial x} + \frac{\partial \rho v}{\partial y} = 0, \tag{16}$$

$$\rho\left(\frac{\partial u}{\partial t} + u\frac{\partial u}{\partial x} + v\frac{\partial u}{\partial y}\right) = -\frac{\partial p}{\partial x}, \tag{17}$$

$$\rho\left(\frac{\partial v}{\partial t} + u\frac{\partial v}{\partial x} + v\frac{\partial v}{\partial y}\right) = -\frac{\partial p}{\partial y}, \tag{18}$$

$$\rho\left(\frac{\partial T}{\partial t}+u\frac{\partial T}{\partial x}+v\frac{\partial T}{\partial y}\right)=\frac{1}{RePr}\frac{\partial}{\partial x_j}\left(\frac{\partial T}{\partial x_j}\right), \tag{19}$$

$$p=\frac{RT_0}{V^2}\rho T=R'\rho T, \tag{20}$$

where $Pr = c_p\mu/k$, Prandtl number which is a finite value, is an intrinsic property of the fluid, not of the flow, whereas $Re = LV\rho_0/\mu$, Reynolds number which is infinity for inviscid flows, and $R' = RT_0/V^2$ is a constant. Hence, the non-dimensional energy equation, Eq.(19), becomes

$$\rho\left(\frac{\partial T}{\partial t}+u\frac{\partial T}{\partial x}+v\frac{\partial T}{\partial y}\right)=0. \tag{21}$$

Therefore, Eqs.(16), (17), (18), (21), and (20) consist of the dimensionless equations for continuity, momentum, and energy, and the ideal gas state equation for two-dimensional, inviscid, low Mach number, and parallel flows.

2.4 Linearized Disturbance Equations

Substituting Eq.(1) into the above five dimensionless equations with the assumption that $\bar{v}(y) = 0, \bar{u}(y) = U(y)$, $p(x, y, t) \approx$ *constant*, and $\bar{p}(y) =$ *constant*, we obtain the linearized disturbance equations as follows.

Continuity:

$$\frac{\partial(\bar{\rho}+\rho')}{\partial t}+\frac{\partial(\bar{\rho}+\rho')(\bar{u}+u')}{\partial x}+\frac{\partial(\bar{\rho}+\rho')v'}{\partial y}=0.$$

Hence,

$$\frac{\partial\rho'}{\partial t}+\bar{\rho}\frac{\partial u'}{\partial x}+U\frac{\partial\rho'}{\partial x}+v'\frac{\partial\bar{\rho}}{\partial y}+\bar{\rho}\frac{\partial v'}{\partial y}=0. \tag{22}$$

Momentum: x component:

$$\left(\frac{\partial(\bar{u}+u')}{\partial t}+(\bar{u}+u')\frac{\partial(\bar{u}+u')}{\partial x}+v'\frac{\partial(\bar{u}+u')}{\partial y}+v'\frac{\partial v'}{\partial y}\right)(\bar{\rho}+\rho')=-\frac{\partial(\bar{p}+p')}{\partial x}.$$

Hence,

$$\bar{\rho}\frac{\partial u'}{\partial t}+\bar{\rho}U\frac{\partial u'}{\partial x}+\bar{\rho}v'\frac{\partial U}{\partial y}=-\frac{\partial p'}{\partial x}. \tag{23}$$

Momentum: y component:

$$\left(\frac{\partial v'}{\partial t} + (\bar{u} + u')\frac{\partial v'}{\partial x} + v'\frac{\partial v'}{\partial y}\right)(\bar{\rho} + \rho') = -\frac{\partial(\bar{p} + p')}{\partial y}$$

Hence,

$$\bar{\rho}\frac{\partial v'}{\partial t} + \bar{\rho}U\frac{\partial v'}{\partial x} = -\frac{\partial p'}{\partial y}. \tag{24}$$

Energy:

$$(\bar{\rho} + \rho')\left(\frac{\partial(\bar{T} + T')}{\partial t} + (\bar{u} + u')\frac{\partial(\bar{T} + T')}{\partial x} + v'\frac{\partial(\bar{T} + T')}{\partial y}\right) = 0.$$

Hence,

$$\bar{\rho}\frac{\partial T'}{\partial t} + \bar{\rho}U\frac{\partial T'}{\partial x} + \bar{\rho}v'\frac{\partial \bar{T}}{\partial y} = 0. \tag{25}$$

Equation of State:

$$p = R'(\bar{\rho} + \rho')(\bar{T} + T') = R'\bar{\rho}\bar{T} + R'(\bar{\rho}T' + \bar{T}\rho') + R'\rho'T',$$

where $p \approx constant$. Keeping the first-order terms and ignoring the other terms, the ideal gas state linearized disturbance equation becomes

$$\bar{\rho}T' + \bar{T}\rho' = 0. \tag{26}$$

2.5 Eigenfunction Equations

By substituting Eq.(2) into the above five linearized disturbance equations, Eqs.(22), (23), (24), (25), and (26), we obtain the eigenfunction equations for continuity, x and y momentum, energy, and equation of state in the following, respectively:

$$i\tilde{\rho}(\alpha U - \beta) + \tilde{v}\rho' + \rho(\tilde{v}' + \tilde{u}i\alpha) = 0, \tag{27}$$

$$-i\beta\rho\tilde{u} + \rho\tilde{v}U' + \rho U i\alpha\tilde{u} = -i\alpha\tilde{p}, \tag{28}$$

$$-i\beta\rho\tilde{v} + \rho U i\alpha\tilde{v} = -\tilde{p}', \tag{29}$$

$$i(\alpha U - \beta)\rho\tilde{T} + \rho T'\tilde{v} = 0, \tag{30}$$

$$\rho\tilde{T} + T\tilde{\rho} = 0, \tag{31}$$

where the prime $'$ denotes $\frac{d}{dy}$. The quantities U, ρ, and T, all of them functions of y, represent the non-dimensional mean streamwise velocity, density, and temperature, respectively. The quantities $\tilde{\rho}$, $\tilde{u}$, $\tilde{v}$, $\tilde{p}$, and $\tilde{T}$, denote the non-dimensional density, x and y velocity components, pressure, and temperature eigenfunctions, respectively. Note that all of the quantities, including y, are dimensionless. The quantities α and β are the complex streamwise wave number and the temporal frequency, respectively.

3 Pressure and Φ Eigenfunction Equations and Boundary Conditions

From the above non-dimensional linearized eigenfunctions, we can obtain the eigenfunction equation of pressure and then the corresponding boundary conditions. Next, we transform the pressure eigenfunction equation into another eigenfunction Φ. Finally, the infinite physical domain is transformed to a finite computational domain. Both transformations make it easy for us to solve the eigenvalue problems by numerical methods.

3.1 Pressure Eigenfunction Equation and Boundary Conditions

From the above five eigenfunction equations, we can obtain the pressure eigenfunction equation. First, from the continuity and momentum eigenfunction equations, that is, Eqs.(27), (28), and (29), we can eliminate the x and y velocity components to obtain an eigenfunction equation for the pressure and the density only. From Eq.(29), we obtain the eigenfunction equation for the y velocity component as expressed by the pressure eigenfunction:

$$\tilde{v} = -\frac{\tilde{p}'}{\rho i(\alpha U - \beta)}. \tag{32}$$

Differentiating Eq.(32) with respective to y, we have

$$\tilde{v}' = \frac{\rho i(\alpha U - \beta)\tilde{p}'' - \tilde{p}'[\rho' i(\alpha U - \beta) + \rho i U'\alpha]}{\rho^2(\alpha U - \beta)^2}. \tag{33}$$

Then, we substitute Eq.(32) into (28) to eliminate the y velocity component eigenfunction and thus obtain the eigenfunction equation for the x velocity

component as expressed by the pressure eigenfunction:

$$\tilde{u} = -\frac{\alpha\tilde{p}(\alpha U - \beta) + U'\tilde{p}'}{\rho(\alpha U - \beta)^2}. \tag{34}$$

Next, we substitute Eqs.(32), (33), and (34) into (27) to eliminate the x and y velocity component eigenfunctions and we obtain an eigenfunction equation for the pressure and the density only:

$$\tilde{p}'' - \frac{2\alpha U'}{\alpha U - \beta}\tilde{p}' + \tilde{\rho}(\alpha U - \beta)^2 - \alpha^2\tilde{p} = 0. \tag{35}$$

Second, the density eigenfunction in Eq.(35) can be eliminated by using the energy and the ideal gas state eigenfunction equations, Eqs.(30) and (31) respectively. Substituting Eq.(32) into (30) to eliminate the y velocity component eigenfunction, we obtain the eigenfunction equation for the temperature as expressed by the pressure eigenfunction:

$$\tilde{T} = -\frac{T'\tilde{p}'}{\rho(\alpha U - \beta)^2}. \tag{36}$$

Substituting Eq.(36) into (31) to eliminate the temperature eigenfunction, we obtain the eigenfunction equation for the density as expressed by the pressure eigenfunction:

$$\tilde{\rho} = \frac{T'\tilde{p}'}{(\alpha U - \beta)^2 T}. \tag{37}$$

Finally, we substitute Eq.(37) into (35) to eliminate the density eigenfunction. The pressure eigenfunction equation is derived as

$$\tilde{p}'' - \left(\frac{2\alpha U'}{\alpha U - \beta} - \frac{T'}{T}\right)\tilde{p}' - \alpha^2\tilde{p} = 0. \tag{38}$$

The boundary conditions for the pressure eigenfunction are obtained by considering the asymptotic form of the solutions of the pressure eigenfunction equation, Eq.(38). As $y \to \pm\infty$, the derivatives of the x velocity component and temperature, U' and T', become negligible and Eq.(38) is simplified to:

$$\tilde{p}'' - \alpha^2\tilde{p} = 0. \tag{39}$$

Then, it's solution is

$$\tilde{p} = C_1 e^{\alpha y} + C_2 e^{-\alpha y} = C_1 e^{(\alpha_r + i\alpha_i)y} + C_2 e^{-(\alpha_r + i\alpha_i)y}, \tag{40}$$

where C_1 and C_2 are arbitrary complex constants and without loss of generality, $\alpha_r \geq 0$. The pressure eigenfunction at $y \to \pm\infty$ suggests that the boundary conditions for the pressure eigenfunction behave like

$$y \to +\infty : \ \tilde{p} = C_2 e^{-(\alpha_r + i\alpha_i)y}, \tag{41}$$

$$y \to -\infty : \ \tilde{p} = C_1 e^{(\alpha_r + i\alpha_i)y}, \tag{42}$$

because the solution of the pressure eigenfunction is bounded when $y \to \pm\infty$.

3.2 Φ Eigenfunction Equation and Boundary Conditions

It is not trivial to solve for the pressure eigenfunctions from Eq.(38), as its real and imaginary parts are second-order differential equations with zero boundary conditions for both pressure, Eqs.(41) and (42), and its derivatives at $y \to \pm\infty$. This problem can be overcome by reducing the order of Eq.(38), by transforming the pressure eigenfunction into another eigenfunction Φ using a function similar to the *Riccati* transformation as (e.g. Michalke [20])

$$\tilde{p}(y) \equiv C e^{\int_0^y \Phi(\eta) d\eta}, \tag{43}$$

where C is an arbitrary complex constant. This transformation implies that $\tilde{p}(y = 0) = C$, an unknown complex constant, meaning that the solution is not unique. Thus, from the transformation, Eq.(43), we have

$$\tilde{p}' = C e^{\int_0^y \Phi(\eta) d\eta} \Phi = \tilde{p}\Phi, \ \tilde{p}'' = (\tilde{p}\Phi)' = (\Phi' + \Phi^2)\tilde{p}. \tag{44}$$

Substituting Eq.(44) into the pressure eigenfunction equation, Eq.(38), and deleting the common factor $\tilde{p}$, we obtain the Φ eigenfunction equation:

$$\Phi' + \Phi^2 - \left(\frac{2\alpha U'}{\alpha U - \beta} - \frac{T'}{T} \right) \Phi - \alpha^2 = 0. \tag{45}$$

Since both the Φ eigenfunction and streamwise wave number α are complex whereas the temporal frequency β is real for spatially developing flows, we can split Φ into the real and imaginary parts, respectively:

$$\Phi = \Phi_r + i\Phi_i, \ \alpha = \alpha_r + i\alpha_i. \tag{46}$$

To obtain the governing equations for Φ_r, and Φ_i, we substitute Eq.(46) into Eq.(45) and split the eigenfunction equation into the real and imaginary parts.

Real part:

$$\Phi_r' + \Phi_r^2 - \Phi_i^2 + A\Phi_r - B\Phi_i - \alpha_r^2 + \alpha_i^2 = 0, \tag{47}$$

Imaginary part:

$$\Phi_i' + 2\Phi_r\Phi_i + A\Phi_i + B\Phi_r - 2\alpha_r\alpha_i = 0, \tag{48}$$

where

$$A(y) = \frac{T'}{T} - \frac{2U'[\alpha_r(\alpha_r U - \beta) + \alpha_i^2 U]}{(\alpha_r U - \beta)^2 + (\alpha_i U)^2}, \tag{49}$$

$$B(y) = \frac{2U'\alpha_i\beta}{(\alpha_r U - \beta)^2 + (\alpha_i U)^2}, \tag{50}$$

and $U(y)$ and $T(y)$ represent the dimensionless mean streamwise velocity and temperature, respectively.

The boundary conditions for the Φ_r and Φ_i eigenfunctions can be derived from the boundary conditions for the pressure eigenfunctions, Eqs.(41) and (42), and the transformation, Eq.(43). From Eq.(44), we have $\tilde{p}' = \tilde{p}\Phi$, that is,

$$\tilde{p}'/\tilde{p} = \Phi = \Phi_r + i\Phi_i. \tag{51}$$

Now, from the boundary conditions for the pressure eigenfunctions, Eqs.(41) and (42), we have

$$y \to +\infty : \ \tilde{p}' = -(\alpha_r + i\alpha_i)C_2 e^{-(\alpha_r + i\alpha_i)y} = -(\alpha_r + i\alpha_i)\tilde{p},$$

$$y \to -\infty : \ \tilde{p}' = (\alpha_r + i\alpha_i)C_1 e^{(\alpha_r + i\alpha_i)y} = (\alpha_r + i\alpha_i)\tilde{p},$$

which imply that

$$y \to +\infty : \ \tilde{p}'/\tilde{p} = -(\alpha_r + i\alpha_i), \tag{52}$$

$$y \to -\infty : \ \tilde{p}'/\tilde{p} = \alpha_r + i\alpha_i. \tag{53}$$

From Eqs.(51), (52), and (53), the boundary conditions for the Φ_r and Φ_i eigenfunctions are obtained as

$$y \to +\infty : \ \Phi_r = -\alpha_r, \ \Phi_i = -\alpha_i, \tag{54}$$

$$y \ \to -\infty : \ \Phi_r = \alpha_r, \ \Phi_i = \alpha_i. \tag{55}$$

3.3 Physical Domain to Computational Domain

We can transform the physical domain $y : (-\infty, +\infty)$ to a computational domain $\xi : [-1, 1]$ by using the transformation:

$$\xi = \tanh(s \cdot y), \tag{56}$$

where s is a stretching constant and

$$\tanh x = \frac{\sinh x}{\cosh x} = \frac{e^x - e^{-x}}{e^x + e^{-x}}.$$

Thus, we have

$$y = \frac{1}{2s} \ln \frac{1+\xi}{1-\xi}, \tag{57}$$

$$\frac{d\xi}{dy} = s \sec^2(sy) = s(1-\xi^2), \tag{58}$$

$$\phi'(y) = \frac{d\phi(y)}{dy} = \frac{d\phi(\xi)}{d\xi} \times \frac{d\xi}{dy} = s(1-\xi^2)\dot{\phi}, \tag{59}$$

where $\dot{\phi}$ is defined by $\dot{\phi} \equiv \frac{d\phi}{d\xi}$ and ϕ is any generic quantity, for example, $\Phi_r, \Phi_i, U, T, etc.$

By substituting Eqs.(57) and (59) into the equations for Φ_r, and Φ_i, i.e., Eqs.(47), (48), (49), and (50), the corresponding equations for $\Phi_r(\xi)$ and $\Phi_i(\xi)$ in the computational domain $\xi : [-1, 1]$ are obtained:

$$F(\xi) = 0, \tag{60}$$

$$G(\xi) = 0, \tag{61}$$

where

$$F(\xi) = s(1-\xi^2)\dot{\Phi}_r(\xi) + \Phi_r^2(\xi) - \Phi_i^2(\xi) + A(\xi)\Phi_r(\xi) - B(\xi)\Phi_i(\xi) - \alpha_r^2 + \alpha_i^2, \tag{62}$$

$$G(\xi) = s(1-\xi^2)\dot{\Phi}_i(\xi) + 2\Phi_r(\xi)\Phi_i(\xi) + A(\xi)\Phi_i(\xi) + B(\xi)\Phi_r(\xi) - 2\alpha_r\alpha_i, \quad (63)$$

$$A(\xi) = \frac{s(1-\xi^2)\dot{T}(\xi)}{T(\xi)} - \frac{2s(1-\xi^2)\dot{U}(\xi)[\alpha_r(\alpha_r U(\xi) - \beta) + \alpha_i^2 U(\xi)]}{(\alpha_r U(\xi) - \beta)^2 + (\alpha_i U(\xi))^2}, \quad (64)$$

$$B(\xi) = \frac{2s(1-\xi^2)\dot{U}(\xi)\alpha_i\beta}{(\alpha_r U(\xi) - \beta)^2 + (\alpha_i U(\xi))^2}. \quad (65)$$

From the boundary conditions for the $\Phi_r(y)$ and $\Phi_i(y)$ eigenfunctions, i.e., Eqs. (54) and (55), the corresponding boundary conditions for the $\Phi_r(\xi)$ and $\Phi_i(\xi)$ eigenfunctions on the computational domain $\xi : [-1, 1]$ are obtained:

$$\xi = 1 : \ \Phi_r = -\alpha_r, \ \Phi_i = -\alpha_i, \quad (66)$$

$$\xi = -1 : \ \Phi_r = \alpha_r, \ \Phi_i = \alpha_i, \quad (67)$$

where $\alpha_r \geq 0$.

4 Conditions of x Velocity Component U and Temperature T for Anti-symmetric Solutions of Φ_r and Φ_i Eigenfunctions

The behaviors of Φ_r and Φ_i eigenfunctions are of great interest. If we assume that the solutions of Φ_r and Φ_i eigenfunctions are anti-symmetric, we can derive the necessary conditions for the distribution of the x velocity component U and temperature T. Assuming that both Φ_r and Φ_i are anti-symmetric, we have

$$\Phi_r(\xi) = -\Phi_r(-\xi), \quad (68)$$

$$\Phi_i(\xi) = -\Phi_i(-\xi), \quad (69)$$

$$F(\xi) = F(-\xi) = 0, \quad (70)$$

$$G(\xi) = G(-\xi) = 0. \quad (71)$$

Differentiating Eqs.(66) and (67) with respective to ξ, we have

$$\dot{\Phi}_r(\xi) = \frac{d\Phi_r(\xi)}{d\xi} = \frac{d(-\Phi_r(-\xi))}{d\xi} = -\dot{\Phi}_r(-\xi)(-1) = \dot{\Phi}_r(-\xi), \quad (72)$$

$$\dot{\Phi}_i(\xi) = \frac{d\Phi_i(\xi)}{d\xi} = \frac{d(-\Phi_i(-\xi))}{d\xi} = -\dot{\Phi}_i(-\xi)(-1) = \dot{\Phi}_i(-\xi). \quad (73)$$

4.1 Conditions of Coefficients A and B

By considering the solutions of the eigenfunction equations, Eqs.(70) and (71), and the properties of the anti-symmetry of the Φ_r and Φ_i eigenfunctions, Eqs.(68), (69), (72), and (73), we can obtain the necessary conditions of coefficients A and B. Now, Eq.(70) implies that

$$F(\xi) = s(1-\xi^2)\dot{\Phi}_r(\xi)+\Phi_r^2(\xi)-\Phi_i^2(\xi)+A(\xi)\Phi_r(\xi)-B(\xi)\Phi_i(\xi)-\alpha_r^2+\alpha_i^2 = 0, \tag{74}$$

$$\begin{aligned} F(-\xi) &= s(1-(-\xi)^2)\dot{\Phi}_r(-\xi)+\Phi_r^2(-\xi)-\Phi_i^2(-\xi)+A(-\xi)\Phi_r(-\xi) \\ &\quad -B(-\xi)\Phi_i(-\xi)-\alpha_r^2+\alpha_i^2 = 0. \end{aligned} \tag{75}$$

Substituting Eqs.(68), (69), and (72) into (75), we have

$$F(-\xi) = s(1-\xi^2)\dot{\Phi}_r(\xi)+\Phi_r^2(\xi)-\Phi_i^2(\xi)-A(-\xi)\Phi_r(\xi)+B(-\xi)\Phi_i(\xi)-\alpha_r^2+\alpha_i^2 = 0. \tag{76}$$

And then subtracting Eq.(76) from (74), we obtain

$$[A(\xi)+A(-\xi)]\Phi_r(\xi)-[B(\xi)+B(-\xi)]\Phi_i(\xi) = 0. \tag{77}$$

Similarly, Eq.(71) implies that

$$G(\xi) = s(1-\xi^2)\dot{\Phi}_i(\xi)+2\Phi_r(\xi)\Phi_i(\xi)+A(\xi)\Phi_i(\xi)+B(\xi)\Phi_r(\xi)-2\alpha_r\alpha_i = 0, \tag{78}$$

$$\begin{aligned} G(-\xi) &= s(1-(-\xi)^2)\dot{\Phi}_i(-\xi)+2\Phi_r(-\xi)\Phi_i(-\xi)+A(-\xi)\Phi_i(-\xi) \\ &\quad +B(-\xi)\Phi_r(-\xi)-2\alpha_r\alpha_i = 0. \end{aligned} \tag{79}$$

Substituting Eqs.(68), (69), and (73) into (79), we have

$$G(-\xi) = s(1-\xi^2)\dot{\Phi}_i(\xi)+2\Phi_r(\xi)\Phi_i(\xi)-A(-\xi)\Phi_i(\xi)-B(-\xi)\Phi_r(\xi)-2\alpha_r\alpha_i = 0. \tag{80}$$

And then subtracting Eq.(80) from (78), we obtain

$$[A(\xi)+A(-\xi)]\Phi_i(\xi)+[B(\xi)+B(-\xi)]\Phi_r(\xi) = 0. \tag{81}$$

Because $\Phi_r(\xi) \not\equiv 0$ and $\Phi_i(\xi) \not\equiv 0$, Eqs.(77) and (81) suggest that the conditions of coefficients A and B for the anti-symmetric solutions of Φ_r and Φ_i eigenfunction are as following:

$$A(\xi) = -A(-\xi), \tag{82}$$

$$B(\xi) = -B(-\xi), \tag{83}$$

that is, the coefficients A and B are anti-symmetric with respective to ξ.

4.2 Conditions of x Velocity Component U and Temperature T

From the conditions of coefficients A and B, Eqs.(82) and (83), we can derive the conditions of x velocity component U and temperature T for the anti-symmetric solutions of Φ_r and Φ_i eigenfunction. First, from Eq.(64), we have

$$\begin{aligned} A(-\xi) &= \frac{s(1-(-\xi)^2)\dot{T}(-\xi)}{T(-\xi)} \\ &\quad - \frac{2s(1-(-\xi)^2)\dot{U}(-\xi)[\alpha_r(\alpha_r U(-\xi)-\beta)+\alpha_i^2 U(-\xi)]}{(\alpha_r U(-\xi)-\beta)^2+(\alpha_i U(-\xi))^2}, \end{aligned}$$

that is,

$$A(-\xi) = \frac{s(1-\xi^2)\dot{T}(-\xi)}{T(-\xi)} - \frac{2s(1-\xi^2)\dot{U}(-\xi)[\alpha_r(\alpha_r U(-\xi)-\beta)+\alpha_i^2 U(-\xi)]}{(\alpha_r U(-\xi)-\beta)^2+(\alpha_i U(-\xi))^2}. \tag{84}$$

Substituting Eqs.(64) and (84) into (82) and considering the independently given distributions of x velocity component U and temperature T, we obtain

$$\frac{\dot{T}(\xi)}{T(\xi)} = -\frac{\dot{T}(-\xi)}{T(-\xi)}, \tag{85}$$

$$\frac{\dot{U}(\xi)[\alpha_r(\alpha_r U(\xi)-\beta)+\alpha_i^2 U(\xi)]}{(\alpha_r U(\xi)-\beta)^2+(\alpha_i U(\xi))^2} = -\frac{\dot{U}(-\xi)[\alpha_r(\alpha_r U(-\xi)-\beta)+\alpha_i^2 U(-\xi)]}{(\alpha_r U(-\xi)-\beta)^2+(\alpha_i U(-\xi))^2}. \tag{86}$$

Second, from Eq.(65), we have

$$B(-\xi) = \frac{2s(1-(-\xi)^2)\dot{U}(-\xi)\alpha_i\beta}{(\alpha_r U(-\xi)-\beta)^2+(\alpha_i U(-\xi))^2},$$

that is,

$$B(-\xi) = \frac{2s(1-\xi^2)\dot{U}(-\xi)\alpha_i\beta}{(\alpha_r U(-\xi)-\beta)^2+(\alpha_i U(-\xi))^2}. \tag{87}$$

Substituting Eqs.(65) and (87) into (83), we obtain

$$\frac{\dot{U}(\xi)}{(\alpha_r U(\xi)-\beta)^2+(\alpha_i U(\xi))^2} = -\frac{\dot{U}(-\xi)}{(\alpha_r U(-\xi)-\beta)^2+(\alpha_i U(-\xi))^2} \tag{88}$$

Therefore, Eqs.(85), (86), and (88) lead to the necessary conditions of x velocity component U and temperature T.

4.3 Condition of x Velocity Component U

By inspecting Eqs.(86) and (88), we find that their denominators should be equal, that is,

$$(\alpha_r U(\xi)-\beta)^2+(\alpha_i U(\xi))^2 = (\alpha_r U(-\xi)-\beta)^2+(\alpha_i U(-\xi))^2.$$

Thus,

$$(\alpha_r^2+\alpha_i^2)(U^2(\xi)-U^2(-\xi)) - 2\alpha_r\beta(U(\xi)-U(-\xi)) = 0,$$

that is,

$$[(\alpha_r^2+\alpha_i^2)(U(\xi)+U(-\xi)) - 2\alpha_r\beta](U(\xi)-U(-\xi)) = 0.$$

Therefore, we obtain two solutions for the x velocity component U:

Solution 1:

$$U(\xi) = U(-\xi), \tag{89}$$

that is, the x velocity component U is symmetric with respective to ξ. Differentiating Eq.(89) with respective to ξ, we have

$$\dot{U}(\xi) = \frac{dU(\xi)}{d\xi} = \frac{dU(-\xi)}{d\xi} = \dot{U}(-\xi)(-1) = -\dot{U}(-\xi). \tag{90}$$

By substituting Eqs.(89) and (90) into (86) and (88), it is found that these two equations happen to be satisfied.

Solution 2:

$$U(\xi) = -U(-\xi) + \frac{2\alpha_r\beta}{\alpha_r^2 + \alpha_i^2}. \tag{91}$$

that is,

$$U(\xi) - \frac{\alpha_r\beta}{\alpha_r^2 + \alpha_i^2} = -\left(U(-\xi) - \frac{\alpha_r\beta}{\alpha_r^2 + \alpha_i^2}\right). \tag{92}$$

If we define

$$H(\xi) = U(\xi) - \frac{\alpha_r\beta}{\alpha_r^2 + \alpha_i^2},$$

then from Eq.(92), we have

$$H(\xi) = -H(-\xi),$$

which suggests that $H(\xi)$ is anti-symmetric with respective to ξ.

Differentiating Eq.(91) with respective to ξ, we have

$$\dot{U}(\xi) = \frac{dU(\xi)}{d\xi} = \frac{d(-U(-\xi))}{d\xi} = -\dot{U}(-\xi)(-1) = \dot{U}(-\xi), \tag{93}$$

By substituting Eqs.(91) and (93) into (86) and (88), it is found that Eq.(86) is satisfied but Eq.(88) is unsatisfied except for the case :

$$\dot{U}(\xi) = \dot{U}(-\xi) = 0, \tag{94}$$

that is, $U(\xi)$ and $U(-\xi)$ are constants. Combining Eqs.(92) with (94), we obtain the required condition of the x velocity component $U(\xi)$:

$$U(\xi) = \frac{\alpha_r\beta}{\alpha_r^2 + \alpha_i^2} + sign(\xi)C, \tag{95}$$

where C is an arbitrary constant such that $U(\xi) > 0$.

Actually, Eq.(94) meets the requirements of Eqs.(86) and (88) and we don't need the constraint of Eq.(91). Therefore, we obtain the condition of the x velocity component $U(\xi)$:

$$\begin{aligned} U(\xi) &= C_+, \qquad \xi > 0, \\ &= C_-, \qquad \xi < 0, \end{aligned} \tag{96}$$

where C_+ and C_- are arbitrary constants. This case is the extreme of the hyperbolic-tangent mean velocity profile when the parameter g is infinity:

$$U(\xi) = e + f\tanh(g\xi),$$

where e, f, and g are constants. For this case, the corresponding equations for $\Phi_r(\xi)$ and $\Phi_i(\xi)$ on the computational domain $\xi : [-1, 1]$ are much simpler. By substituting Eq.(93) into Eqs.(60), (61), (62), (63), (64), and (65), we obtain:

$$s(1-\xi^2)\dot{\Phi}_r(\xi) + \Phi_r^2(\xi) - \Phi_i^2(\xi) + \frac{a(1-\xi^2)\dot{T}(\xi)}{T(\xi)}\Phi_r(\xi) - \alpha_r^2 + \alpha_i^2 = 0, \quad (97)$$

$$s(1-\xi^2)\dot{\Phi}_i(\xi) + 2\Phi_r(\xi)\Phi_i(\xi) + \frac{a(1-\xi^2)\dot{T}(\xi)}{T(\xi)}\Phi_i(\xi) - 2\alpha_r\alpha_i = 0. \quad (98)$$

These two equations don't include the x velocity component $U(\xi)$ and thus it doesn't contribute to the solutions of the equations.

Therefore, the required condition of the x velocity component is that it is symmetric with respective to ξ or Eq.(96).

4.4 Condition of Temperature T

The required condition of the temperature can be derived from Eq.(85). We recall that any function can be decomposed to two parts: even, or symmetric, and odd, or anti-symmetric, functions. So, we decompose the temperature as:

$$T(\xi) = \frac{1}{2}(T(\xi) + T(-\xi)) + \frac{1}{2}(T(\xi) - T(-\xi)) = T_e(\xi) + T_o(\xi), \quad (99)$$

where the even part is $T_e(\xi) = \frac{1}{2}(T(\xi) + T(-\xi))$ and the odd part is $T_o(\xi) = \frac{1}{2}(T(\xi) - T(-\xi))$. Then, we substitute Eq.(99) into Eq.(85) to obtain

$$\frac{\dot{T}_e(\xi) + \dot{T}_o(\xi)}{T_e(\xi) + T_o(\xi)} = -\frac{\dot{T}_e(-\xi) + \dot{T}_o(-\xi)}{T_e(-\xi) + T_o(-\xi)} = \frac{\dot{T}_e(\xi) - \dot{T}_o(\xi)}{T_e(\xi) - T_o(\xi)}, \quad (100)$$

where we have used the properties of even and odd functions and their derivatives from Eqs.(72) and (90). Therefore, from Eq.(100), we have

$$(\dot{T}_e(\xi) + \dot{T}_o(\xi))(T_e(\xi) - T_o(\xi)) = (T_e(\xi) + T_o(\xi))(\dot{T}_e(\xi) - \dot{T}_o(\xi)),$$

which can be simplified to

$$T_e\dot{T}_o = T_o\dot{T}_e. \tag{101}$$

The solutions of Eq.(101) can be divided into three cases:

1. $T_o \equiv 0$. Obviously, Eq.(101) is satisfied. This case means that the temperature is an even function, that is,

$$T(\xi) = T(-\xi). \tag{102}$$

2. $T_e \equiv 0$. Obviously, Eq.(101) is satisfied. This case means that the temperature is an odd function. But, we know that the temperature must be positive; therefore, we reject this solution.

3. $T_e \not\equiv 0$ and $T_o \not\equiv 0$. Then,

$$\frac{\dot{T}_e}{T_e} = \frac{\dot{T}_o}{T_o} = \frac{dT_o}{T_o d\xi} = \frac{d(\ln T_o)}{d\xi} = \frac{d(\ln T_e)}{d\xi}. \tag{103}$$

   Therefore, $d(\ln T_o) = d(\ln T_e)$, i.e.,

$$T_o = T_e^C, \tag{104}$$

   where $C = constant$. But, T_o is odd and T_e even. Therefore, Eq.(104) doesn't have solutions.

In summary, the necessary conditions of anti-symmetric solutions are that both the temperature T and the x velocity component U are symmetric with respective to ξ or Eq.(96). Furthermore, these conditions are sufficient; therefore, they are the sufficient and necessary conditions for Φ to have anti-symmetric solutions.

4.5 Conditions of x Velocity Component U and Temperature T in the Physical Domain

We can transform the anti-symmetric solutions of Φ_r and Φ_i and these sufficient and necessary conditions from the computational domain into the physical domain. Substituting the transformation Eq.(56), $\xi = \tanh(sy)$,

which is an odd function of the variable y, into Eqs.(68), (69), (89), (96), and (102), we obtain

$$\Phi_r(\tanh(sy)) = \Phi_r(\xi) = -\Phi_r(-\xi) = -\Phi_r(-\tanh(sy)) = -\Phi_r(\tanh(-sy)), \tag{105}$$

$$\Phi_i(\tanh(sy)) = \Phi_i(\xi) = -\Phi_i(-\xi) = -\Phi_i(-\tanh(sy)) = -\Phi_i(\tanh(-sy)), \tag{106}$$

$$U(\tanh(sy)) = U(\xi) = U(-\xi) = U(-\tanh(sy)) = U(\tanh(-sy)), \tag{107}$$

$$\begin{aligned} U(y) &= C_+, \qquad y > 0, \\ &= C_-, \qquad y < 0, \end{aligned} \tag{108}$$

$$T(\tanh(sy)) = T(\xi) = T(-\xi) = T(-\tanh(sy)) = T(\tanh(-sy)), \tag{109}$$

which suggest that in the physical domain, the solutions of Φ_r and Φ_i are also anti-symmetric and the sufficient and necessary conditions are that both the temperature and the x velocity component are symmetric with respective to y.

5 Numerical Results and Discussions

Using Eqs.(60) and (61) with the corresponding boundary conditions, Eqs.(66) and (67), we can solve for the Φ eigenfunction. Next, using the transformation equations, Eqs.(57) and (39), and the Φ eigenfunction, we can obtain the pressure eigenfunction. Finally, we use the pressure eigenfunction and Eqs. (34), (32), (37), and (36) to obtain the x and y velocity component, density, and temperature eigenfunctions, respectively.

5.1 Numerical Methods for Solving Φ_r and Φ_i Eigenfunctions

Eigenfunction equations, Eqs.(60) and (61), with the corresponding boundary conditions, Eqs.(64) and (65), can be solved numerically by the shooting method for the initial value problems [34]. Any non-dimensional velocity and temperature profiles can be specified as input to the stability calculation; in particular, either analytic functions or the computed laminar profiles can be used. For example, the analytical expressions that typify flames in shear layers, such as the hyperbolic tangent function, have been used in Michalke's

analysis [20]. For the spatially developing flows, we specify the value of β (real) and an initial guessed value of α (complex) and integrate the above two equations from $\xi = -1$ to 0 and from $\xi = 1$ to 0. The solutions are matched at $\xi = 0$ by adjusting the value of α leading to different boundary conditions for Φ at $\xi = 1$ and $\xi = -1$. The change of Φ is determined by the Newton iteration method. Convergent solutions of Φ_r and Φ_i eigenfunctions are obtained when the change of α is less than 10^{-7}. The shooting method is reasonably fast and each run only takes a few minutes on a Pentium 500 MHz machine.

The set of equations for instability eigenfunctions, both real and imaginary parts, can also be solved together with the eigenvalues using an iterative scheme. The 'TWOPNT' program written by Sandia [32] is used for construction of such a scheme. A set of arbitrary guessed values for eigenvalues and eigenfunctions are prescribed as the initial values for the TWOPNT program. TWOPNT performs Newton iterations and in the event of a failure, time marching is carried out to provide a better guessed. The procedure is repeated until a convergent solution is found. Usually, the program converges within only a few minutes on a Linux PC (Pentium II 500 MHz) for each specified α value. However, due to the uncertainty in the initial profiles for the eigenfunctions, the iterative scheme may not find a convergent solution. Both the shooting method and the iterative scheme will be validated by comparison of results obtained with current codes and those obtained by Michalke [20] for a temporally developing mixing layer. A hyperbolic tangent profile is prescribed for the stream-wise velocity with constant temperature. In a temporal developing mixing layer, the spatial wave perturbation is assigned α (real) and the frequency β (complex) is the eigenvalue to be solved. Both real and imaginary parts of β are solved for; however, only the imaginary part is of interest as it determines the growth of perturbation as function of time.

5.2 Solutions of Pressure Eigenfunction

After obtaining the solutions of Φ_r and Φ_i eigenfunctions, we can obtain the solution of pressure eigenfunction by using the transformations (57) and (39). From Eq.(58), we have

$$dy = \frac{d\xi}{s(1-\xi^2)}$$

Substituting it into Eq.(39) , we have

$$\tilde{p}(y) = C_3 e^{\int_\infty^y \Phi(\eta) d\eta} + C_4, \tag{110}$$

where C_3 and C_4 are constants. The integration was carried out in the computational domain from $\xi = 1$ to a certain point corresponding to y. As the stability equation for the pressure eigenfunction is linear, any C_3 and C_3 can satisfy the governing equation. We simply set C_3 =1 and C_4=0.

5.3 Validation of Shooting Method and TWOPNT

We have performed calculations to validate both the shooting code and the iterative scheme using TWOPNT by comparing results obtained for a temporally developing mixing layer investigated by Michalke [20]. Table 1 summarizes the comparison and the current results using both shooting method and TWOPNT are within 0.3% of those by Michalke [20].

Table 1 Comparison of Most Amplified Frequencies ($\omega \equiv \beta_i/\alpha$)

α	ω_{TWOPNT}	$\omega_{shooting}$	$\omega_{Michalke}$
0.2	0.3479	0.3485	0.3487
0.4	0.2353	0.2350	0.2352
0.5	0.1876	0.1880	0.1875
0.6	0.1442	0.1440	0.1442
0.8	0.0673	0.0671	0.0672

In Figure 1, current results of the imaginary part of frequency, β_i, versus wave number (real) are compared to those obtained by Michalke [20] showing excellent agreement. We further check the code to see if antisymmetric solutions are obtained with a symmetric velocity profile in a spatially developing flow. A nonreacting laminar jet with a velocity profile prescribed by $U = exp(-y^2/2)$ is used for this purpose. Figure 2 presents the computed values of $-\alpha_i$ versus frequency showing a peak value located around 0.3. The corresponding real part is presented in Figure 3 indicating a near linear relation between α_r and β. Figure 4 shows the computed results of real and imaginary parts of eigenfunction Φ. The results are clearly anti-symmetric as

found theoretically in a previous section. The corresponding real and imaginary parts of pressure eigenfunction are plotted in Figure 5 and Figure 6 respectively. It is interesting to note that both are symmetric with respective to y=0 as the eigenfunction $\Phi(y)$ is antisymmetric. The magnitude of pressure eigenfunction can be multiplied or added by any constant as the stability equation is linear. Of importance is the relative magnitude between the real and imaginary parts.

5.4 Results of Triple Flames

Detailed procedures and equations used for solving triple flames are described by Chen and Echekki [33]. Shown in Figure 7 is a typical contour profile of reaction rate for a triple flame under gravity pointed downward. As seen in the figure, the triple flame has developed into a unstable mode with large variation in the transverse direction. The normalized frequency estimated from the numerical simulation is about 0.083 for a triple with Froude number of 2. The Froude number, $Fr = S_L^2/gW$, is based on planar premixed laminar flame speed, S_L, and the inlet mixing width, W. We have performed linear stability analysis using results from steady triple flames under various degrees of gravity effect.The planar premixed flame speed, the mixing width, and the free-stream properties, such as temperature and density, are used for normalization of governing equations.The computed velocity and temperature profiles are first fitted by analytical functions of the forms $U(y) = a \cdot exp(-b \cdot y^2) + c \cdot tanh(d \cdot y)$ and $T(y) = e \cdot exp(-f \cdot y^2)$, where a, b, c, d, e, and f are coefficients determined by least square fitting. Next, these fitted functions are input to the shoot method program for linear stability analysis. We found that the iterative scheme using TWOPNT often cannot find the convergent solutions due to poor initial guessed values for the eigenfunctions. Therefore, the results reported below were obtained using the shooting method.

The computed results for the negative imaginary part of wave number, $-\alpha_i$, versus frequency are presented in Figure 8. These results were based on velocity and temperature profiles at $3\frac{1}{3}$ mixing widths downstream of the triple flame tip with two different Froude numbers and zero gravity. The results show that as gravity effect increases (with Froude decreasing), the frequency at the most amplified mode moves toward higher value and so is the mag-

nitude. That is, increasing gravity effect leads to less stable flames; this is consistent with numerical simulations of triple flames. The location of most amplified frequency is found around 0.073 (i.e., $0.46/2\pi$) for the case of Fr=2 which is very close to the frequency (0.083) seen in the numerical simulations [33]. This good agreement is perhaps coincident as the most amplified frequency changes with axial location. Figure 9 shows similar results but at a slightly further downstream location of 5 mixing widths. The magnitude of $-\alpha_i$ are seen to be lower than those at $3\frac{1}{3}$ W but the peak location of $-\alpha_i$ remains about the same. Figure 10 shows the computed eigenfunction Φ. As both the velocity and temperature are symmetric with respective to y, the eigenfunction, Φ, is antisymmetric with respective to y. The corresponding pressure eigenfunction is plotted in Figure 11 showing symmetric profiles with respective to y as expected.

6 Summary

A linear stability analysis has been carried out for triple flames using computed velocity and temperature profiles. Detailed linear stability equations are derived and analyzed for the special case of symmetric profiles. It is found that the pressure eigenfunction is symmetric under this condition. Two computer programs have been constructed using the shooting method and the TWOPNT software which is an iterative method. For temporally developing flows, we found that both methods are accurate for predicting the linear instability characteristics. However, for spatially developing flows, the iterative scheme using TWOPNT is more difficult to use and sometimes it never converges due to the poor initial guess of eigenfunctions. The difficulties may be overcome in the future by using an initial guess obtained from the shooting method. Applications to triple flames were conducted using the shooting method. The results show that gravity effect influences the stability of the triple flames. When gravity is pointed toward the direction in which the triple flame propagating, increasing gravity effect leads to less stable flames. More importantly, the frequency of most amplified mode is found to be close to that observed in numerical results of a unstable triple flame. The present analysis is found useful in interpreting the computed unstable modes seen in the numerical simulations.

References

[1] Phillips H 1965 *10th Int. Symp. on Combustion* (Pittsburgh, PA: Combustion Institute) pp. 1227–1283.

[2] Buckmaster J and Matalon M 1988 22nd Int. Symp. on Combustion pp. 1527–1535.

[3] Hartley L J and Dold J W 1991 Flame propagation in a nonuniform mixture: analysis of a propagating triple flame, *Combust. Sci. and Tech.* **80** 23–46.

[4] Chung S H and Lee B J 1991 On the characteristics of laminar lifted flames in a nonpremixed jet, *Combust. Flame* **86** 62–72.

[5] Kioni P N, Rogg B, Bray K N C, and Liñán A 1993 Flame spread in laminar mixing layers: the triple flame, *Combust. Flame* **95** 276–290.

[6] Lee B J, Kim J S, and Chung S H 1994 *25th Int. Symp. on Combustion* (Pittsburgh, PA: Combustion Institute) pp. 1175–1181.

[7] Lee B J and Chung S H 1997 Stabilization of Lifted Tribrachial flames in a laminar nonpremixed Jet, *Combust. Flame* **109** 163–172.

[8] Ruetsch G R, Vervisch L and Liñán A 1995 Effects of Heat Release on Triple Flames, *Phys. Fluids* **7(6)** 1447–1454.

[9] Ruetsch G R and Ferziger J H 1996 Lewis number effects on partially premixed flames, *Annual Research Briefs* Center for Turbulence Research NASA Ames/Stanford University, pp. 67–84.

[10] Domingo P and Vervisch L 1996 *26th Int. Symp. on Combustion* (Pittsburgh, PA: Combustion Institute) pp. 233.

[11] Plessing T, Terhoeven P, Peters N, and Mansour M S 1998 An experimental and numerical study of a laminar triple flame *Combust. Flame* **115** 335–353.

[12] Daou J and Liñán A 1998 The role of unequal diffusivities in ignition and extinction fronts in strained mixing layers, *Combust. Theo. Model.* **2** 449–477 .

[13] Echekki T and Chen J H 1998 Structure and propagation of methanol-air triple flames, *Combust. Flame* **114** 231–245.

[14] Ghosal S and Vervisch L 2000 Theoretical and numerical study of a symmetrical triple flame using the parabolic flame path approximation accepted by *J. Fluid Mechanics*.

[15] Chen Y C and Bilger R W 2000 Stabilization mechanisms of lifted flames in axisymmetric jet flows, accepted by *Combust. Flame*.

[16] Im H G and Chen J H 1999 Structure and propagation of triple flames in partially premixed hydrogen-air mixture, *Combust. Flame* **119** 436–454.

[17] Shin, D.S. and Ferziger, J.H., "linear stability of the reacting mixing layer," AIAA Journal, vol. 29, no 10, pp. 1634-1642, 1991.

[18] Rayleigh, Lord, "On the Stability, or Instability, of Certain Flow Motions," Proceedings of the London Math. Soc. Vol. 11, 1880, pp.57-70.

[19] Lin, C. C., The Theory of Hydrodynamic Stability, Cambridge Univ. Press, Cambridge, England, UK, 1995.

[20] Michalke, A, "On the Inviscid Instability of the Hyperbolic Tangent Velocity Profile," Journal of Fluid Mechanics, Vol. 19, pp. 543-556, 1964.

[21] Monkewitz, P. A., and Huerre, P., " Influence of the Velocity Ratio on the Spatial Instability of Mixing Layers," Physics of fluids, Vol. 25, July 1982, pp. 1137-1143.

[22] Morkovin, M.V., " Guide to Experiments on Instability and Laminar-Turbulent Transition in Shear Layers," NASA Ames short course,1998.

[23] Koochesfahani, M. M., and Frieler, C.E., " Inviscid Instability Characteristics of Free Shear Layer with Non-Uniform Density," AIAA Paper 87-0047, Jan. 1987.

[24] Kimura, I., " Stability of Laminar Jet Flames," Tenth Symposium(International) on Combustion. The Combustion Inst., Pittsburgh. PA, 1965, pp. 1295-1300.

[25] Trouve, A., and Candel, S. M., " Linear Stability of the Inlet Jet in Ramjet Dump Combustor," AIAA Paper 88-0149, Jan,1988.

[26] Jackson, T. L., and Grosch, C. E., " Effect of Heat Release on the Spatial Stability of a Supersonic Reacting Mixing Layer," NASA CR-181753, Nov.1988.

[27] Mahalingam, S., Cantwell, B., and Ferziger, J., " Effects of Heat Release on the Structure and Stability of a Coflowing, Chemically Reacting Jet," AIAA Paper 89-0691, Jan.1989.

[28] Groppengiesser, H., " Study on the Stability of Boundary Layers in Compressible Fluids," NASA TT F-12, 786. Feb. 1970.

[29] Blumen, W., Drazin,P. G., and Billings, D.F., " Shear Layer Instability of an Inviscid Compressible Fluid. Part 2," Journal of Fluid Mechanics, Vol.71, Sept. 1975, pp. 305-316.

[30] Sandham,N., and Reynolds, W., " The Compressible Mixing Layer: Linear Theory and Direct Simulation," AIAA Paper 89-0371. Jan.1989.

[31] Buckmaster J and Peters N 1988 The infinite candle and its stability-a paradigm for flickering diffusion flames, *21st Symp. (Int.) on Combustion* (Pittsburgh, PA: Combustion Institute) pp. 1829–1836.

[32] Grcar, J.F., "The TWOPNT Program for Boundary Value Problems," Sandia Report, SAND91-8230, 1992.

[33] Chen J Y and Echekki T 1999 Numerical study of buoyancy and differential diffusion effects on the structure and dynamics of triple flames *Proceedings of the Fifth Int. Microgravity Combustion Workshop, NASA/CP report 1999–208917* pp. 427–430.

[34] Drazin, P.G., and Reid, W.H., Hydrodynamic Stability. Cambridge Univ. Press, Cambridge, England, UK, 1982. pp. 129-132.

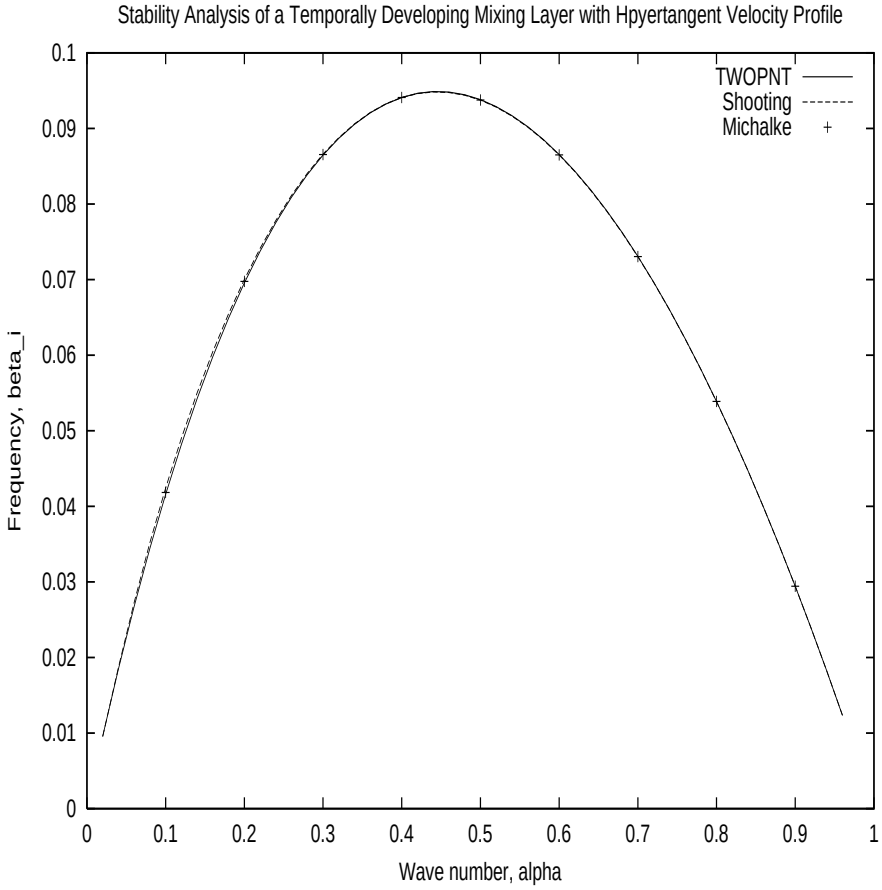

Figure 1: Comparison of most amplified frequency (imaginary part) computed by TWOPNT and shooting method against those obtained by Michalke [20].

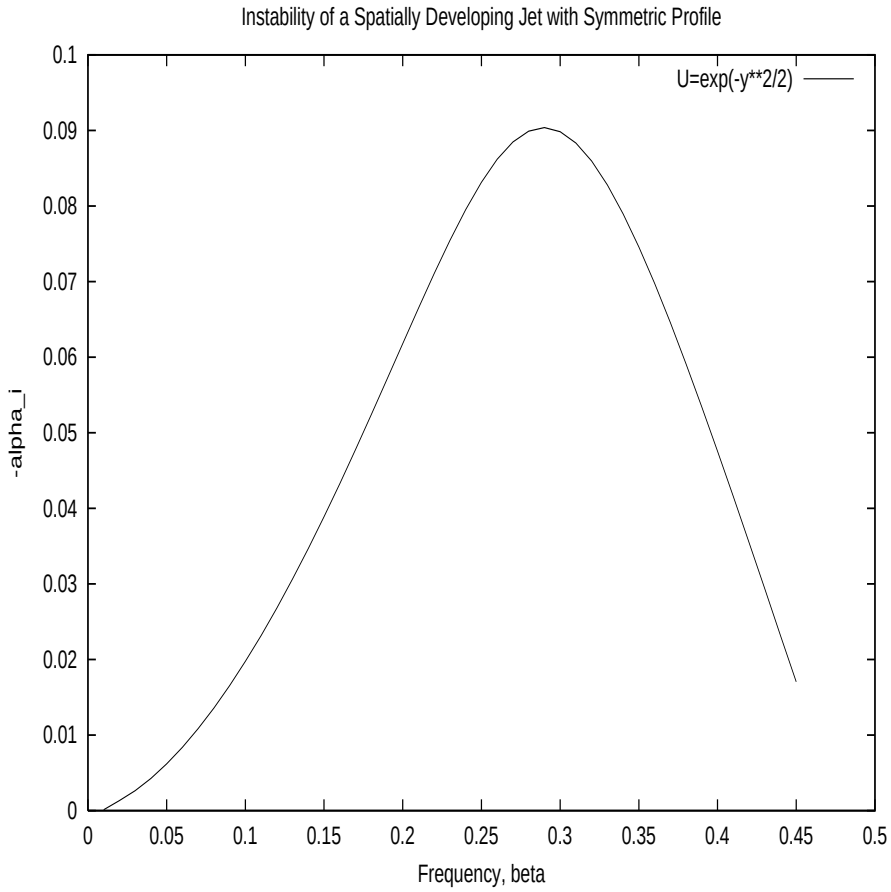

Figure 2: Results of the negative imaginary part of wave number, $-\alpha_i$, versus frequency for a nonreacting laminar jet with a symmetric velocity profile $U = exp(-y^2/2)$.

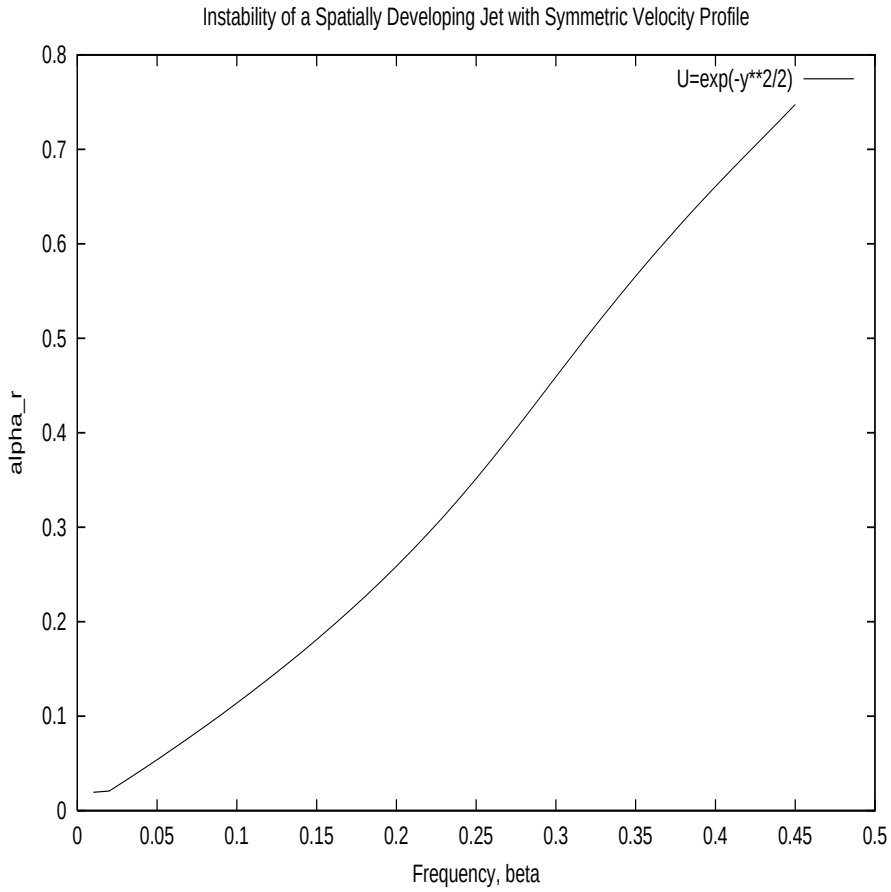

Figure 3: Results of the real part of wave number, α_r, versus frequency for a nonreacting laminar jet with a symmetric velocity profile $U = exp(-y^2/2)$.

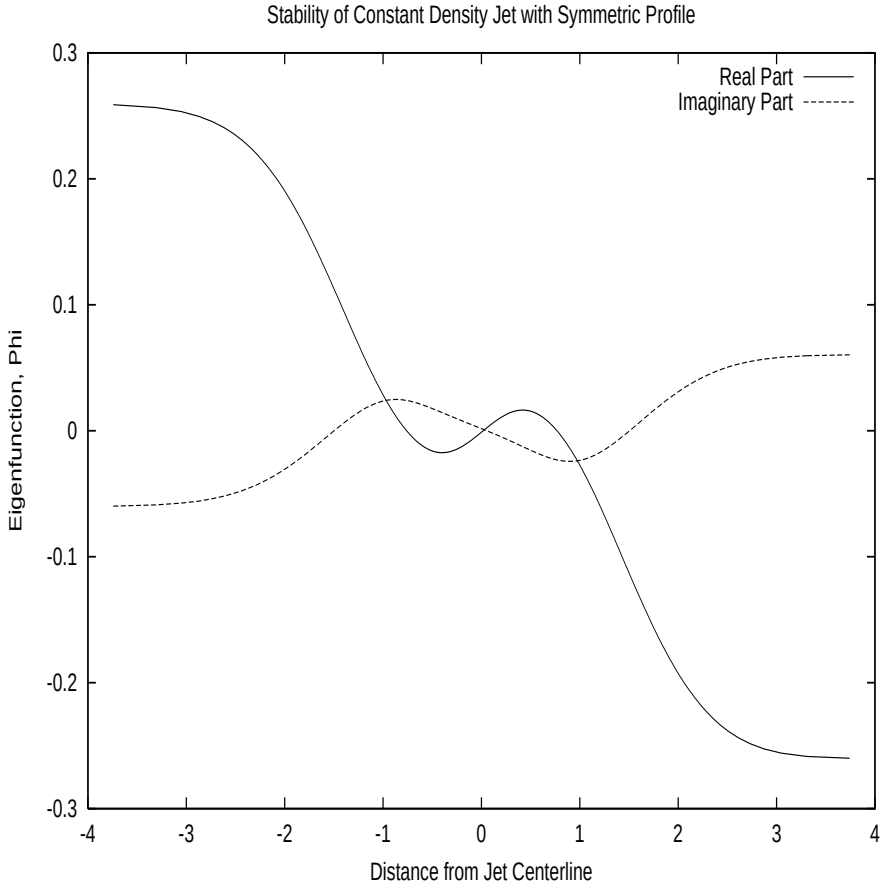

Figure 4: Results of eigenfunction Φ versus distance from jet centerline for a nonreacting laminar jet with a symmetric velocity profile $U = exp(-y^2/2)$.

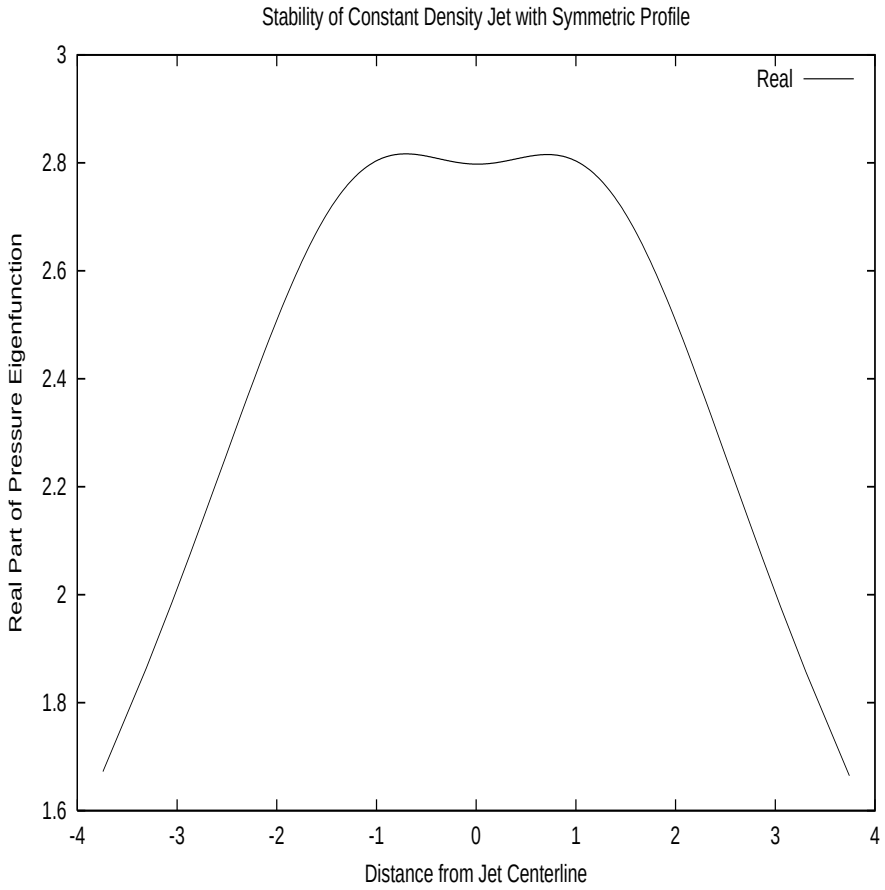

Figure 5: Results of real part of pressure eigenfunction versus distance from jet centerline for a nonreacting laminar jet with a symmetric velocity profile $U = exp(-y^2/2)$.

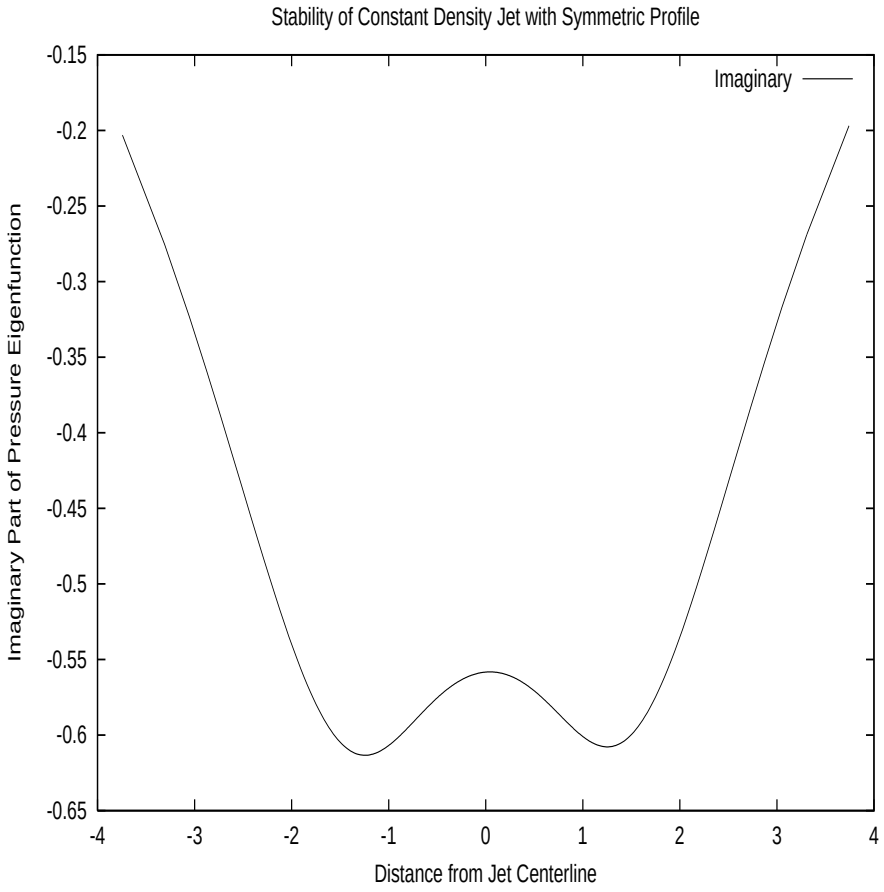

Figure 6: Results of imaginary part of pressure eigenfunction versus distance from jet centerline for a nonreacting laminar jet with a symmetric velocity profile $U = exp(-y^2/2)$.

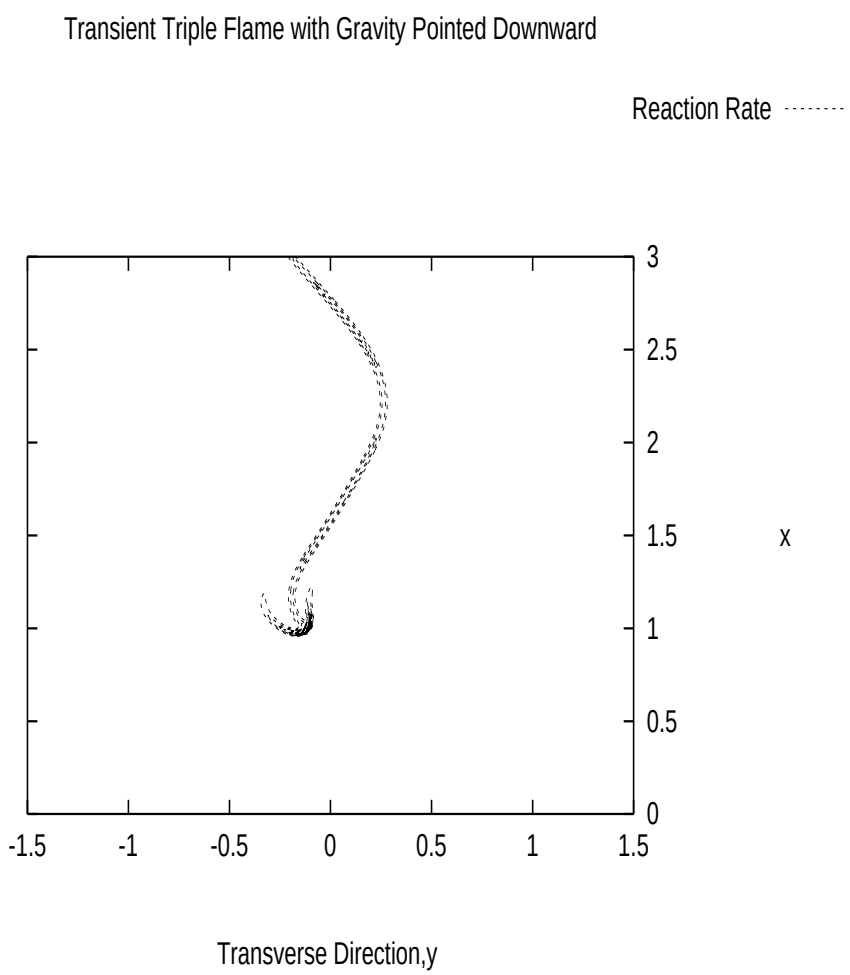

Figure 7: Computed contour of reaction rate for a unstable triple flame under gravity pointed downward showing large variation in transverse direction.

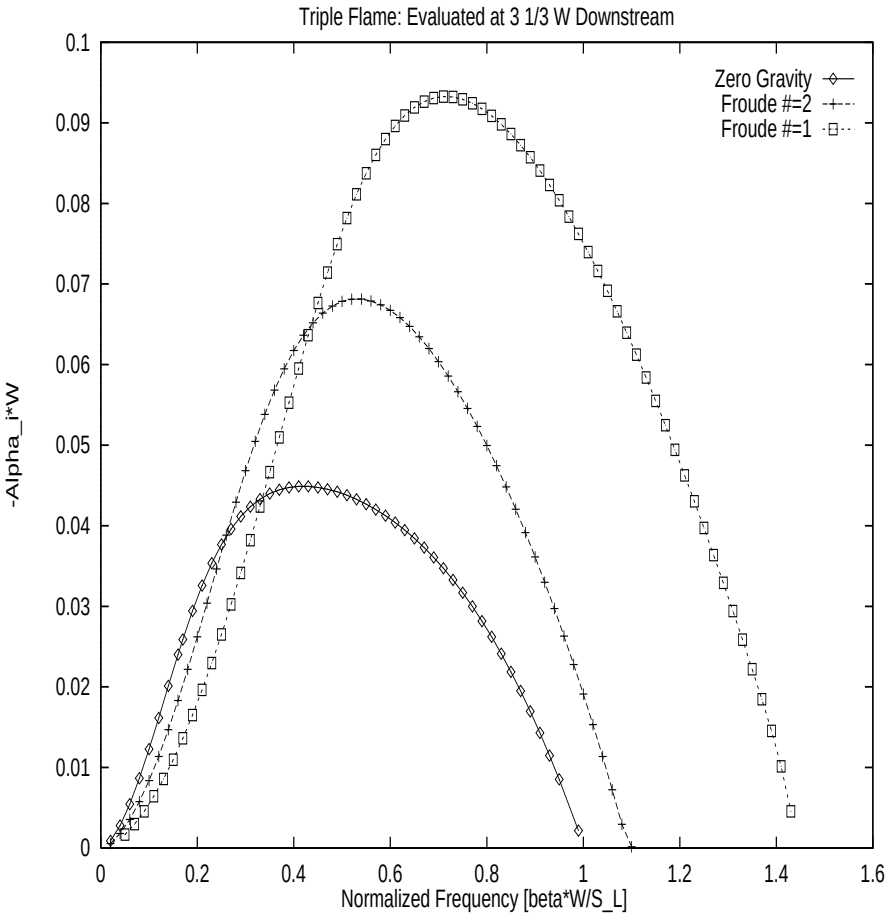

Figure 8: Computed values of the negative wave number, $-\alpha_i$, for stable triple flames under various degree of gravity effect at a downstream location of 3 1/3 W.

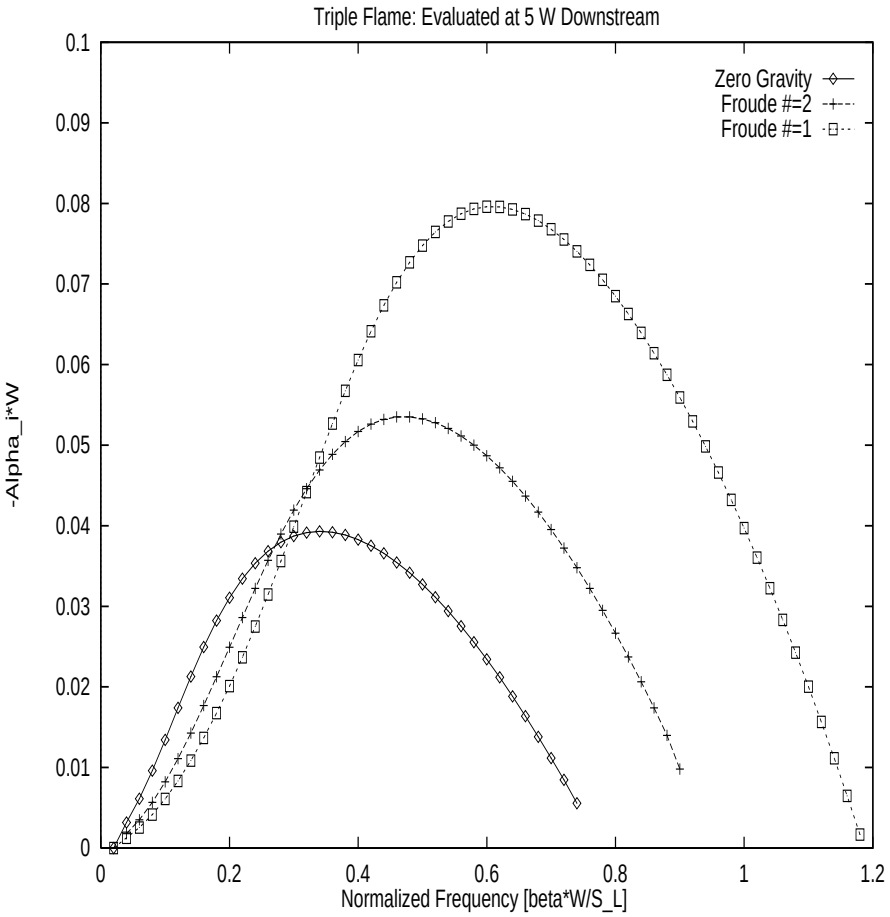

Figure 9: Computed values of the negative wave number, $-\alpha_i$, for stable triple flames under various degree of gravity effect at a downstream location of 5 W.

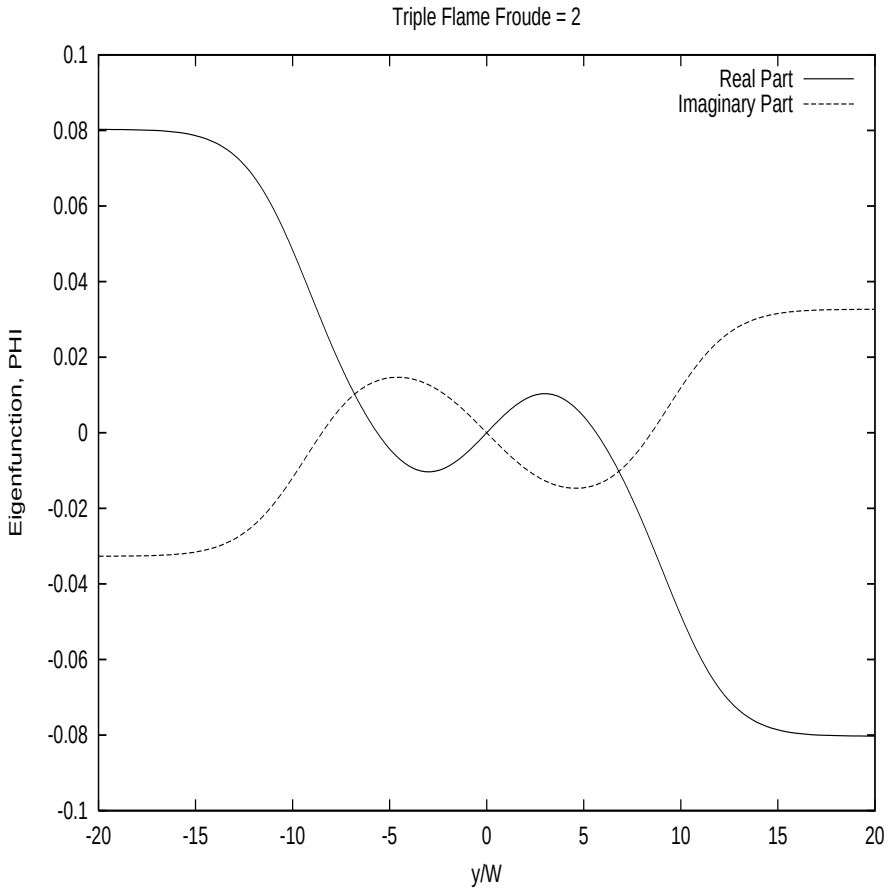

Figure 10: A typical eigenfunction Φ for a stable triple flame with Fr=2 at a downstream location of 45 W.

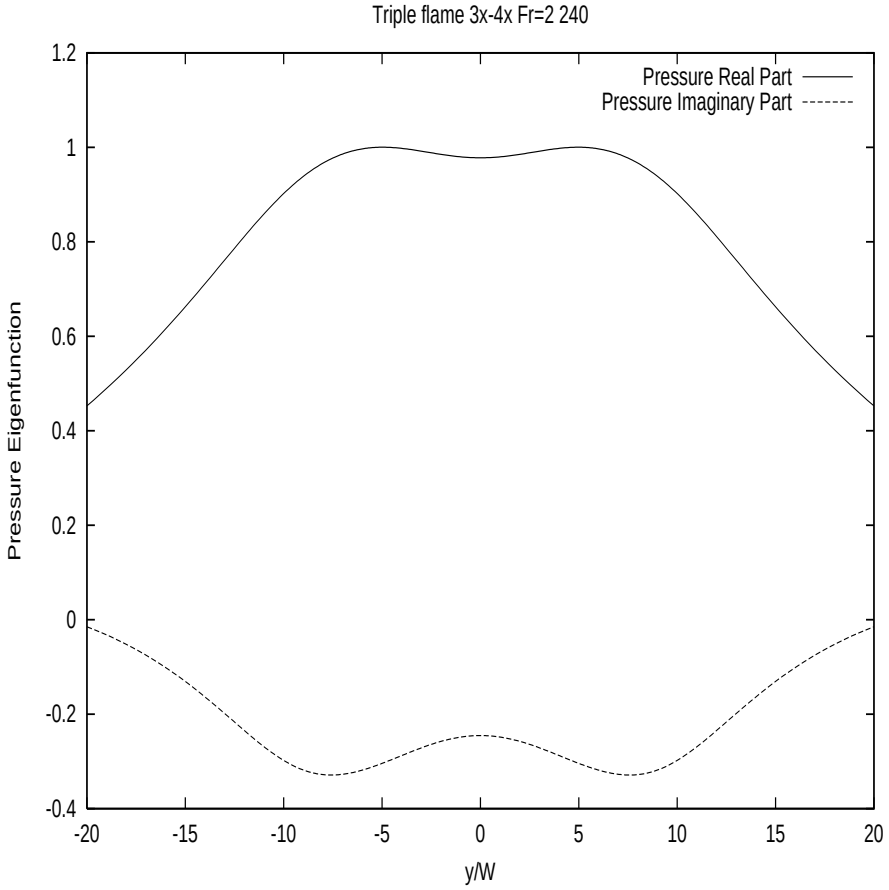

Figure 11: A typical pressure eigenfunction for a stable triple flame with Fr=2 at a downstream location of 45 W.